
Probability-Generating Function Kernels for Spherical Data

Theodore Papamarkou¹ Alexey Lindo²

Abstract

Probability-generating function (PGF) kernels are introduced, which constitute a class of kernels supported on the unit hypersphere, for the purposes of spherical data analysis. PGF kernels generalize RBF kernels in the context of spherical data. The properties of PGF kernels are studied. A semi-parametric learning algorithm is introduced to enable the use of PGF kernels with spherical data.

1. Introduction

This paper contributes to spherical data analysis by developing a new class of kernels, called probability-generating function (PGF) kernels. By construction, PGF kernels are supported on the unit hypersphere, making them a natural choice for spherical data.

PGF kernels are dot-product kernels. Furthermore, PGF kernels generalize radial basis function (RBF) kernels, and therefore the former are expected to have better predictive performance on spherical data than the latter.

Contribution. A summary of contributions follows. PGF kernels are introduced as compositions of PGFs. This way, another connection between machine learning and probability is drawn. It is shown that PGF kernels generalize RBF kernels. A semi-parametric learning algorithm is introduced to fit PGF kernels to spherical data. PGF kernels are equipped with a notion of depth and width, both of which are explored via an ablation study. Three examples are presented to demonstrate the applicability of PGF kernels, namely two Gaussian process (GP) regression examples on circular and spherical data, and a deep kernel learning (DKL) classification example on higher-dimensional spherical data.

Comparison with other works. Daniely et al. (2016) have

¹Department of Mathematics, The University of Manchester, Manchester, United Kingdom ²School of Mathematics and Statistics, University of Glasgow, Glasgow, United Kingdom. Correspondence to: Theodore Papamarkou <theo.papamarkou@manchester.ac.uk>, Alexey Lindo <alexey.lindo@glasgow.ac.uk>.

studied theoretical aspects of compositional kernels based on generating functions (GFs), with an emphasis on the duality between GF kernels and (neural network) activation functions. In contrast, this paper focuses on PGF kernels (rather than GF kernels), studying their properties and relation to other kernels, and introducing a learning algorithm that enables the use of PGF kernels in practice. Liang & Tran-Bach (2021) have focused on a subclass of PGF kernels, based on compositions of a single PGF, and have introduced a learning algorithm for this subclass by drawing a link between kernels and activation functions. In contrast, this paper defines PGF kernels in their generality, allowing compositions of different PGFs, and puts forward a learning algorithm that allows the use of PGF kernels as a standalone entity, without necessitating a link with activation functions.

Paper structure. Section 2 highlights related work in the literature. Section 3 introduces PGF kernels, studies their properties and relations with other kernels, and provides examples of kernels based on known PGFs. Section 4 introduces a learning algorithm to fit PGF kernels to spherical data, and uses this algorithm for GP regression and DKL classification. The paper concludes with a discussion, providing directions for future work (section 5).

2. Related Work

Spherical data analysis. Spherical data analysis refers to the analysis of data supported on a hypersphere. Numerous methods have been developed for spherical data analysis. Lei et al. (2019) have introduced a neural network architecture and a spherical convolutional kernel, the latter being used as a component of the former. The approach of Lei et al. (2019) is designed for point cloud data in \mathbb{R}^3 , which are typically processed using spherical regions. Marques et al. (2022) have applied GP regression to approximate incident radiance functions on the sphere in \mathbb{R}^3 . Several works have focused on the development of kernels on a hypersphere. Guinness & Fuentes (2016) have studied the differentiability properties of kernels on a hypersphere. Pennington et al. (2015) have introduced a method to approximate polynomial kernels for data on the unit sphere using random spherical Fourier features. Zhao & Song (2018) have proposed a power series expansion of the RBF kernel for heat diffusion on a hypersphere.

PGFs. A PGF is defined as

$$g(s) := \sum_{i=0}^{\infty} p_i s^i, \quad (1)$$

where $p_i \in [0, 1]$, $i = 0, 1, 2, \dots$, is a sequence of probabilities. It is assumed that $\sum_{i \geq 0} p_i \leq 1$, and therefore the power series in equation 1 converges absolutely for all $|s| \leq 1$ (Grimmett & Stirzaker, 2020). PGFs were introduced by De Moivre in 1730 (Seal, 1949; Fischer, 2011). Nowadays, PGFs are widely used in branching processes, theory of random walks, renewal theory, and analytic combinatorics.

Compositional kernels. Composition of kernels is a common operation in practice. Python packages, such as `GPYTORCH` (Gardner et al., 2018), provide functionality and examples of kernel composition. The term ‘compositional kernel’ is also linked to the more topical class of kernels investigated by Daniely et al. (2016); Liang & Tran-Bach (2021), establishing a duality between kernels and activation functions. This paper has its methodological origin in the topical notion of compositional kernels (Daniely et al., 2016; Liang & Tran-Bach, 2021), but it shifts the attention away from their duality with activation functions. In doing so, this paper is thus focused on the general operation of kernel composition, introducing a methodological and computational framework to compose kernels using PGFs.

GPs and DKL. Section 4 relies on GPs and DKL. The log-marginal likelihoods used for GP regression and GP classification (as part of DKL) are available in Rasmussen & Williams (2005, equation 2.30) and Milios et al. (2018), respectively. For DKL, the reader is referred to Wilson et al. (2016).

3. PGF Kernels

This section introduces PGF kernels, their relations to other kernels, and their properties. It also provides examples of PGF kernels based on known PGFs. Hereafter, $\rho(x, z) := \langle x, z \rangle$ denotes the correlation between $x \in \mathbb{S}^h$ and $z \in \mathbb{S}^h$, where $\langle \cdot, \cdot \rangle$ is the dot product and $\mathbb{S}^h := \{x \in \mathbb{R}^{h+1} : \|x\| = 1\}$ is the unit h -sphere with $h \geq 1$.

3.1. Definition

Definition 3.1 introduces PGF kernels. PGF kernels apply compositions of PGFs on the correlation of their inputs.

Definition 3.1. Let g_1, \dots, g_n be PGFs and $\rho(x, z)$ the correlation between $x \in \mathbb{S}^h$ and $z \in \mathbb{S}^h$. The n -depth PGF kernel $\mathcal{K}[g_1, \dots, g_n]$ is defined as

$$\mathcal{K}[g_1, \dots, g_n](x, z) := g_n \circ \dots \circ g_1(\rho(x, z)). \quad (2)$$

Setting $g = g_1 = \dots = g_n$ in equation 2 yields the special

case

$$\mathcal{K}[(g)_n](x, z) := \mathcal{K}[\underbrace{g, \dots, g}_{n \text{ times}}](x, z). \quad (3)$$

Equation 3 yields the n -fold composition of g , which is also known as the n -fold iteration of g and is commonly denoted by $g_{(n)}$. $\mathcal{K}[(g)_n]$ represents the PGF kernel defined by iterations of a single PGF, previously referred to as compositional kernel in Liang & Tran-Bach (2021). The composition $g_n \circ \dots \circ g_1$ of different PGFs g_1, \dots, g_n is known in the literature on branching processes as an iterated function system in varying or random environment (Kozlov, 1977; Kersting & Vatutin, 2017; Alsmeyer, 2021), but it has not been used in machine learning problems. Definition 3.1 introduces PGF kernels as compositions of different PGFs g_1, \dots, g_n .

Definition 3.2 introduces the notions of layer and layer width for PGF kernels. This way, PGF kernels have layers, depth and width, similarly to neural networks.

Definition 3.2. Let $\mathcal{K}[g_1, \dots, g_n]$ be a PGF kernel. The i -th PGF g_i is called the i -th compositional layer or, shortly, the i -th layer of the kernel. The number l_i of non-zero terms in the series expansion of PGF g_i (see equation 1) is called the width of the i -th layer.

An n -depth PGF kernel $\mathcal{K}[g_1, \dots, g_n]$ is parameterized by the coefficients of its PGFs g_1, \dots, g_n . Note that each layer width l_i can be finite or infinite. If all layer widths (l_1, \dots, l_n) are finite, then the kernel contains $\sum_{i=1}^n l_i$ parameters. If at least one of the layer widths is infinite, then the kernel contains an infinite number of parameters.

3.2. Relations to Common Kernels

PGF kernels are dot-product kernels. A dot-product kernel $g(\rho(x, z))$ entails an arbitrary function g (Smola et al., 2001), while a PGF kernel employs a composition $g_n \circ \dots \circ g_1$ of PGFs as g . In fact, a composition $g_n \circ \dots \circ g_1$ of PGFs is a PGF. So, a PGF kernel is a dot-product kernel for which g is a PGF. This remark clarifies that a PGF kernel can alternatively be defined as $g(\rho(x, z))$, where g is a PGF; instead, definition 3.1 is chosen to emphasize the role of compositional depth in machine learning problems.

RBF kernels are PGF kernels. In other words, each RBF kernel can be expressed as $g(\rho(x, z))$, where g is a PGF.

Proposition 3.3. *RBF kernels are PGF kernels.*

Proof. Consider the RBF kernel

$$K(x, z) = \exp\left(-\frac{1}{2\sigma^2}\|x - z\|^2\right), \quad (4)$$

where σ is the scalelength. Recall the polarization identity:

$$\|x - z\|^2 = \|x\|^2 + \|z\|^2 - 2\langle x, z \rangle. \quad (5)$$

Since $\|x\| = \|z\| = 1$, it follows from equation 5 that

$$\|x - z\|^2 = 2(1 - \langle x, z \rangle). \quad (6)$$

Combining equations 4 and 6 yields

$$K(x, z) = \exp\left(\frac{1}{\sigma^2}(\rho(x, z) - 1)\right). \quad (7)$$

By expanding the exponential function as a power series around the correlation, equation 7 becomes

$$K(x, z) = \sum_{i=0}^{\infty} p_i \rho^i(x, z), \quad (8)$$

$$p_i = \exp\left(-\frac{1}{\sigma^2}\right) \frac{1}{i! \sigma^{2i}}. \quad (9)$$

Equation 8 is a PGF kernel if and only if for any $j \in \mathbb{N} \cup \{0\}$ it holds that $0 \leq p_i \leq 1$ and $\sum_{i=0}^{\infty} p_i = 1$. It is obvious from equation 9 that $p_i > 0$. Moreover, combining equations 7 and 8 gives

$$\sum_{i=0}^{\infty} p_i \rho^i(x, z) = \exp\left(\frac{1}{\sigma^2}(\rho(x, z) - 1)\right),$$

and setting $\rho(x, z) = 1$ leads to $\sum_{i=0}^{\infty} p_i = 1$, whence it follows that $p_i \leq 1$. \square

Polynomial kernels with positive coefficients summing up to one are PGF kernels. In reverse, PGF kernels with a finite number of positive coefficients are polynomial kernels. It follows directly from these observations that neither polynomial kernels nor PGF kernels are subsumed by each other.

3.3. Properties

Proposition 3.4 establishes the fact that PGF kernels are positive-definite and expresses their eigensystem in closed form. Proposition 3.4 is a special case of the corresponding proposition of Smola et al. (2001) for the eigensystem of dot-product kernels.

Proposition 3.4. *Let $\mathcal{K}[g_1, \dots, g_n] : \mathbb{S}^h \times \mathbb{S}^h \rightarrow [-1, 1]$ be a PGF kernel.*

1. $\mathcal{K}[g_1, \dots, g_n]$ is positive-definite on $\mathbb{S}^h \times \mathbb{S}^h$.
2. The eigenfunctions of $\mathcal{K}[g_1, \dots, g_n]$ are the spherical harmonic functions Y_{ij} of degree $i \in \{0\} \cup \mathbb{N}$ and of order $j = 1, \dots, r(h, i)$, with associated eigenvalues

$$\lambda_{ij} = \frac{2p_i \pi^{h/2}}{\Gamma(h/2) r(h, i)}$$

of multiplicity

$$r(h, i) = \frac{2i + h - 2}{i} \binom{i + h - 3}{i - 1}.$$

p_i are the probabilities of the PGF $g_n \circ \dots \circ g_1$ and Γ is the Gamma function.

Proof. Since \mathcal{K} is a PGF kernel, it is a dot-product kernel. This allows to invoke Smola et al. (2001), which completes the proof. \square

As stated in proposition 3.5, PGF kernels are rotationally stationary, which means that they are stationary with respect to rotations about the origin. In the present context, rotations are bijections that preserve the origin and spherical distance. PGF kernels are rotationally stationary due to the fact that the correlation $\rho(x, z)$ between two points x and z corresponds to the cosine of the angle between x and z , as elaborated in the proof of proposition 3.5.

Proposition 3.5. *PGF kernels are rotationally stationary.*

Proof. Let \mathcal{K} be a PGF kernel. The dot product between the inputs x and z of \mathcal{K} is given by $\langle x, z \rangle = \|x\| \|z\| \cos \theta$, where θ denotes the angle between x and z . Since $\|x\| = \|z\| = 1$, it follows that $\rho(x, z) = \cos \theta$. Let x' and z' be rotations of x and z . Due to the applied rotation, the angle between x' and z' is θ . Thus, $\rho(x', z') = \rho(x, z)$, and therefore $\mathcal{K}(x, z) = \mathcal{K}(x', z')$ according to equation 2. \square

Proposition 3.5 generalizes to dot-product kernels. More generally, rotational stationarity is a common property for other kernel families operating on spherical data.

PGF kernels based on PGFs that map perfectly correlated spherical data to one are correlation kernels (see proposition 3.6). In other words, such kernels map any two points into $[-1, 1]$, and any two perfectly correlated points to one.

Proposition 3.6. *Let g_1, \dots, g_n be PGFs. If for each $i = 1, \dots, n$, the PGF g_i satisfies $g_i(1) = 1$, then the PGF kernel $\mathcal{K}[g_1, \dots, g_n]$ is a correlation kernel.*

Proof. Let x and z be two points on the unit sphere \mathbb{S}^h . For any PGF g_i , $i = 1, \dots, n$, it holds that $|g_i(s)| \leq 1$, $s \in [-1, 1]$. Furthermore, the correlation function satisfies $|\rho(x, z)| \leq 1$. Thus, $|\mathcal{K}[g_1, \dots, g_n](x, z)| \leq 1$. It is assumed that $g_i(1) = 1$ for all $i = 1, \dots, n$. Since $\rho(x, x) = 1$, it follows that $\mathcal{K}[g_1, \dots, g_n](x, x) = 1$. \square

3.4. Kernels Based on Known PGFs

A PGF can be expressed as an infinite series according to equation 1 or as a closed-form function. Consequently, the resulting PGF kernel is expressed as an infinite series or as a closed-form function. In this subsection, common PGFs are used to provide examples of PGF kernels in closed form. Such examples are provided to spark interest for future research, as PGF kernels arising from common PGFs have not been studied.

Two possible ways to classify PFGs and the resulting PGF kernels are based on the existence of explicit PGF iterations and the number of non-zero terms in the series expansion of equation 1. First, two classes of PGFs are induced, depending on whether the PGFs have explicit iterations. The resulting PGF kernels are said to satisfy the closure property if the corresponding PGFs have explicit iterations. Second, PGFs without explicit iterations can have a finite or infinite series expansion, whereas PGFs with explicit iterations have an infinite series expansion. Thus, PGF kernels satisfying the closure property are not polynomial kernels.

Two examples of PGF kernels that do not satisfy the closure property are based on binomial and Poisson PGFs, hereafter termed binomial and Poisson kernels. The lack of closure property implies that binomial and Poisson kernels can not be expressed in closed form, and are therefore approximated numerically.

In what follows, PGF kernels that arise from compositions of Harris, linear fractional and θ kernels are discussed. As a prerequisite, appendix A recaps on the definitions of Harris, linear fractional and θ PGFs. Appendix B states and proves the closure and other properties of some of these kernels.

Definition 3.7. Let $\rho(x, z)$ be the correlation between $x \in \mathbb{S}^h$ and $z \in \mathbb{S}^h$. The Harris kernel with parameters c and r is defined as

$$\mathcal{H}_{c,r}(x, z) := (c\rho(x, z)^{-r} - (c - 1))^{-\frac{1}{r}}, \quad (10)$$

where $r \in \mathbb{N}$ and $c > 1$.

Definition 3.8. Let $\rho(x, z)$ be the correlation between $x \in \mathbb{S}^h$ and $z \in \mathbb{S}^h$. The linear fractional kernel with parameters a and b is defined as

$$\mathcal{F}_{a,b}(x, z) := 1 - (a(1 - \rho(x, z))^{-1} + b)^{-1}, \quad (11)$$

where $a > 0$, $b > 0$, and $a + b \geq 1$.

Table 5 in appendix B shows all nine possible cases of PGF kernels that arise from n -fold iterations of the nine cases of θ PGFs (see definition A.3 in appendix A). Note that the PGF kernels based on θ PGFs generalize linear fractional kernels, since the latter are derived from the first three cases of Table 5 by setting $\theta = 1$. A PGF kernel that arises from the n -fold composition of θ PGFs is considered in propositions 3.9 and 3.10. This kernel and its infinite-depth version can be expressed in closed form according to propositions 3.9 and 3.10, respectively (the proofs are available in appendix B). The PGF kernel appearing in propositions 3.9 and 3.10 is qualitatively different from Harris and linear fractional kernels, because it arises from a composition, rather than an iteration, of θ PGFs.

Proposition 3.9. Consider the n -depth PGF kernel $\mathcal{T}_{\theta,c}[g_1, \dots, g_n]$ that arises from the n -fold composition of

θ PGFs $g_i(s) = 1 - ((1 - s)^{-\theta} + c_i)^{-1/\theta}$, where $c_i > 0$ for $i = 1 \dots, n$. This kernel expresses as

$$\mathcal{T}_{\theta,c}[g_1, \dots, g_n](x, z) = 1 - ((1 - \rho(x, z))^{-\theta} + c)^{-1/\theta}, \quad (12)$$

where $c = \sum_{i=1}^n c_i$.

Proposition 3.10. The infinite-depth limit of the PGF kernel of proposition 3.9 is given by

$$\lim_{n \rightarrow \infty} \mathcal{T}_{\theta,c}[g_1, \dots, g_n](x, z) = 1 - ((1 - \rho(x, z))^{-\theta} + c)^{-\frac{1}{\theta}}, \quad (13)$$

where $c = \sum_{i=1}^{\infty} c_i$.

All the PGF kernels mentioned in subsection 3.4 are correlation kernels. However, arbitrary PGF kernels, as used in learning tasks (section 4), are not necessarily correlation kernels.

4. Learning with PGF Kernels

This section introduces a learning algorithm to fit PGF kernels to spherical data (subsection 4.1). The proposed algorithm is put in use to run GP regression (subsection 4.2) and DKL classification (subsection 4.3).

4.1. Learning Algorithm

Fitting a model equipped with a PGF kernel to a dataset, involves learning the kernel parameters, which are the PGF coefficients. In practice, the number of PGF parameters is reduced by introducing a numerical approximation to ensure numerical stability and computational tractability. Consider an n -depth PGF kernel $\mathcal{K}[g_1, \dots, g_n]$ with layer widths (l_1, \dots, l_n) . Each PGF g_i is numerically approximated by a series truncation. More concretely, the first $m_i < \infty$ terms are maintained in the series expansion of PGF g_i , where $m_i \leq l_i$. So, the numerical approximation of PGF kernel $\mathcal{K}[g_1, \dots, g_n]$ contains $m = \sum_{i=1}^n m_i$ parameters. In this paper, (m_1, \dots, m_n) are referred to as (truncation) widths.

Typically, kernels are used in Bayesian non-parametrics. While PGF kernels are suitable for non-parametric modeling, they contain more parameters than other kernels. From this perspective, numerical approximations of PGF kernels introduce a semi-parametric setup.

To learn the m PGF kernel parameters, stochastic optimization is run on a set of corresponding real-valued parameters. More concretely, at each iteration of the optimization algorithm, a gradient descent step is taken in the space of real-valued parameters, which are then transformed to approximate PGF coefficients via the softmax function in order to evaluate the loss function.

4.2. GP Regression

4.2.1. CIRCULAR VON MISES DENSITY

This subsection provides examples based on the circular von Mises density $f : \mathbb{S}^1 \rightarrow [0, \infty)$ given by

$$f(x|\kappa, \mu) = \frac{\exp(\kappa \cos(x - \mu))}{2\pi I_0(\kappa)},$$

where κ and μ correspond to the shape and location parameters, and $I_0(\kappa)$ denotes the modified Bessel function of the first kind of order zero. In the experiments, the von Mises density parameters are set to $\kappa = 2$ and $\mu = (0, 0)^T$. Two GP regression examples related to the circular von Mises density are presented, namely an ablation study of PGF kernel width and depth, and a performance comparison between PGF and other kernels.

The ablation study aims to demonstrate the role of width and depth in the predictive performance of PGF kernels. To this end, two sets of comparisons are run. To assess the role of width, three single-layer PGF kernels with increasing width $m_1 = 2$, $m_1 = 100$ and $m_1 = 200$ are compared. To assess the role of depth, three fixed-width PGF kernels with increasing depth $n = 1$, $n = 2$ and $n = 3$ are compared; more specifically, the widths are set to $m_1 = 10$, $(m_1, m_2) = (10, 10)$ and $(m_1, m_2, m_3) = (10, 10, 10)$.

A training set is simulated by drawing 250 samples from the circular von Mises density and adding Gaussian noise $\mathcal{N}(\mu = 0, \sigma = 0.5)$ to them. For each PGF kernel, a GP regression model is fitted to the training set by running the Adam optimizer for the same number of iterations (200). The standard log-marginal likelihood function for GP regression is used; see [Rasmussen & Williams \(2005, equation 2.30\)](#). A test set of 250 data points is drawn from the circular von Mises density. Using the estimated PGF kernel parameters obtained from training, predictions are made on the known ground truth, that is, on the noiseless test set.

Figure 1 visualizes the relative predictive performance of PGF kernels of varying width or depth. The blue line in each plot represents the underlying circular von Mises density. The orange points on the bottom right plot and the pink points on the top right plot correspond to the noisy training set and the noiseless test set. The red points in the other plots of Figure 1 depict predictions. The first three plots in row one correspond to single-layer PGF kernels with widths $m_1 = 2$, $m_1 = 100$ and $m_1 = 200$, while the first three plots in row two correspond to fixed-width PGF kernels with depths $n = 1$, $n = 2$ and $n = 3$. As can be seen from the first and second rows of plots, increasing the width or depth produces predictions (red points) in closer proximity to the test set (pink points in the top right plot). In other words, Figure 1 shows that increasing the width or depth of a PGF kernel results in higher predictive performance.

Table 1. Error metrics (MAE and MSE) demonstrate the effect of PGF kernel width and depth on predictive performance for GP regression fitted to data drawn from the circular von Mises density. Increasing the width or depth reduces these error metrics and therefore improves predictive performance.

SINGLE LAYER, VARYING WIDTH		
WIDTH	MAE	MSE
2	2.8564	11.8405
100	1.3331	2.7496
200	0.5144	0.4973
FIXED WIDTH, VARYING DEPTH		
DEPTH	MAE	MSE
1	2.8576	11.9041
2	1.4035	3.1663
3	0.2530	0.1082

Table 1 summarizes numerically the predictive performance of the simulation visualized in Figure 1. More specifically, two error metrics are reported, namely the mean absolute error (MAE) and the mean squared error (MSE). As observed, both MAE and MSE are strictly decreasing functions of width and depth.

Next, a predictive performance comparison is made between the PGF kernel and other well-known kernels. In this example, the PGF kernel with depth $n = 3$ and widths $(m_1, m_2, m_3) = (30, 30, 30)$ is used. Thus, the employed PGF kernel has $m = 90$ parameters. The comparison is carried out against the RBF, Matern, periodic and spectral mixture kernel.

Ten training sets, each consisting of 500 data points, are simulated following the sampling procedure described in the ablation study. For each kernel, a GP regression model is fitted to each training set by running the Adam optimizer for the same number of iterations (1,000). The adopted log-marginal likelihood function is mentioned in [Rasmussen & Williams \(2005, equation 2.30\)](#). Ten test sets, each consisting of 500 data points, are drawn from the circular von Mises density. For each kernel, predictions are made and error metrics are computed on each test set.

Table 2 summarizes numerically the predictive performance based on the kernels under comparison. For each kernel, the mean MAE and mean MSE across the ten test sets are tabulated. For these means, standard errors are also reported. In this GP regression experiment, the PGF kernel attains lower MAE and MSE than the RBF kernel. This is an empirical confirmation of the fact that PGF kernels generalize RBF kernels (see proposition 3.3). Besides, the PGF kernel yields the smallest means and standard errors for MAE and MSE in comparison to the other kernels used in the experiment.

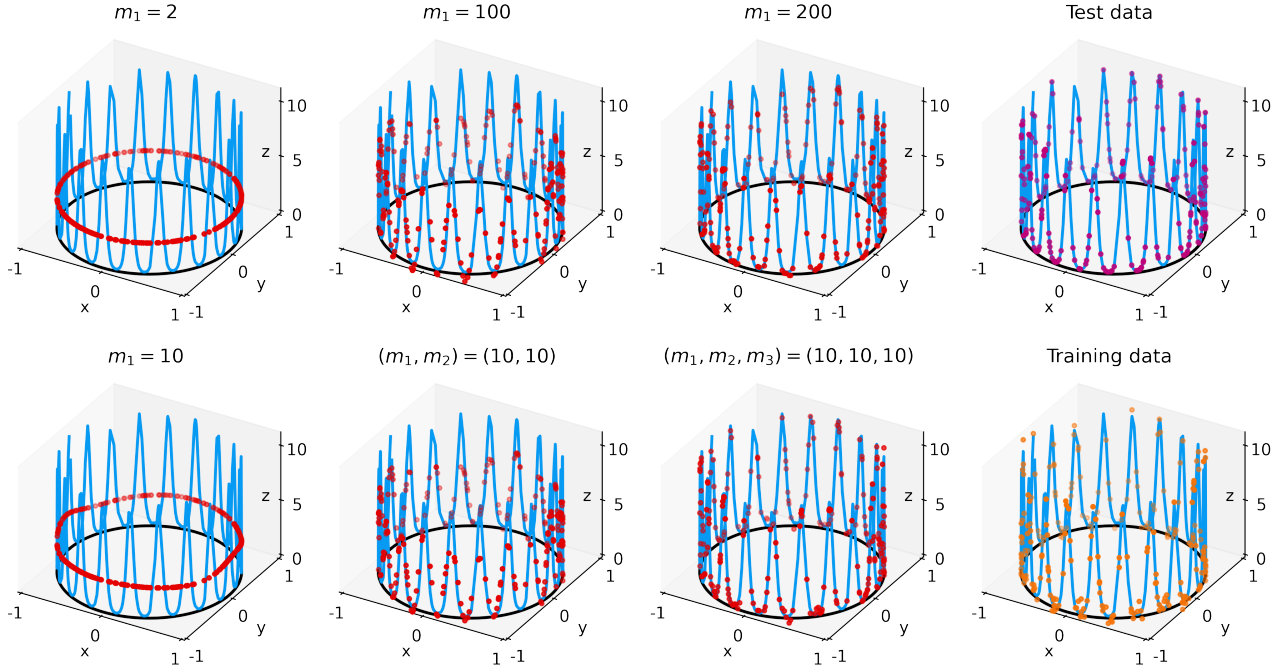


Figure 1. Visual demonstration of the effect of PGF kernel width and depth on predictive performance for GP regression fitted to data drawn from the circular von Mises density. The blue line represents the circular von Mises density from which the data are simulated. The orange, pink and red points represent training data, test data and predictions, respectively. Increasing the width or depth brings the predictions (red points) closer to the test data (pink points) and therefore improves predictive performance.

Table 2. Mean MAEs and MSEs (accompanied by standard errors) for GP regression fitted to data, drawn from the circular von Mises density, using PGF, RBF, Matern, periodic and spectral mixture kernels. For each kernel, the error metric means and standard errors are obtained from ten runs (for details, see the main text). Metrics reported in bold indicate best performance.

KERNEL	MAE	MSE
PGF	0.1683 ±0.0181	0.0501 ±0.0122
RBF	1.3144±1.3583	4.5370±5.7027
MATERN	0.3766±0.0360	0.2621±0.0669
PERIODIC	0.3031±0.0265	0.1748±0.0289
SPECTRAL	0.2553±0.0328	0.1170±0.0360

4.2.2. SPHERICAL EXPONENTIAL-COSINE FUNCTION

This subsection provides an example based on spherical input data living on S^2 and output data simulated from an exponential-cosine (exp-cos) function. More concretely, points on the sphere are simulated in polar coordinates (θ, ϕ) , where θ and ϕ denote the polar angle and azimuthal angle, respectively. The polar coordinates are transformed to Cartesian coordinates, and the latter constitute the input data. The output data are generated from the spherical exp-cos function $f : [0, \pi] \times [-\pi, \pi] \rightarrow [0, \infty)$ given by

$$f(\theta, \phi) = \exp\left(u \sum_{i=1}^4 \cos(v(a_i\theta + b_i\phi + c_i))\right), \quad (14)$$

where $(a_1, a_2, a_3, a_4) = (0, 1, 1, 1)$, $(b_1, b_2, b_3, b_4) = (1, 1, 0, 1)$, $(c_1, c_2, c_3, c_4) = (0, \pi/2, \pi, 3\pi/2)$, $u = 0.5$ and $v = 15$.

A predictive performance comparison is made between the PGF kernel and the RBF, Matern, periodic and spectral mixture kernel. In this example, the PGF kernel with depth $n = 3$ and widths $(m_1, m_2, m_3) = (20, 20, 20)$ is used, which has $m = 60$ parameters.

Four training sets, each consisting of 5,000 data points, are generated. For each training set, 5,000 input data points are simulated by sampling uniformly at random the polar angle θ and azimuthal angle ϕ . The corresponding output data points are generated by evaluating the exp-cos function of equation 14 at the input data points and by adding Gaussian noise $\mathcal{N}(\mu = 0, \sigma = 0.2)$. For each kernel, a GP regression model is fitted to each training set by running the Adam optimizer for the same number of iterations (1,000). The adopted log-marginal likelihood function is available in [Rasmussen & Williams \(2005, equation 2.30\)](#). Four noiseless test sets, each consisting of 5,000 data points, are generated similarly to the training sets, the only difference being that noise is not added to the output. The test sets are generated without noise to ensure that predictive performance is evaluated against the known ground truth given by equation 14. For each kernel, predictions are made and error metrics are computed on each test set.

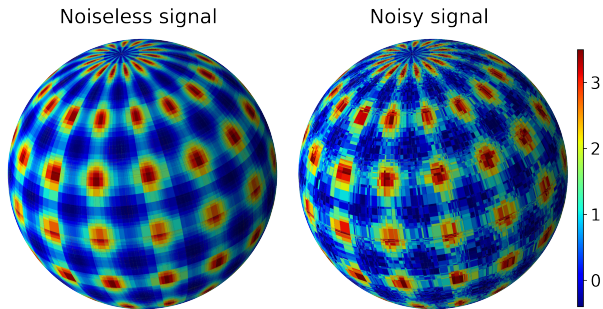


Figure 2. Noiseless (left) and noisy version (right) of the spherical exp-cos function given by equation 14. For the noisy version, Gaussian noise $\mathcal{N}(\mu = 0, \sigma = 0.2)$ is added to the exp-cos function. Training sets are drawn from such noisy realizations, whereas test sets are drawn from the noiseless version of the exp-cos function.

Table 3. Mean MAEs and MSEs (accompanied by standard errors) for GP regression fitted to data, drawn from the spherical exp-cos function (equation 14), using PGF, RBF, Matern, periodic and spectral mixture kernels. For each kernel, the error metric means and standard errors are obtained from four runs (for details, see the main text). Metrics reported in bold indicate best performance.

KERNEL	MAE	MSE
PGF	0.1476 ±0.0076	0.0443±0.0085
RBF	0.3094±0.1598	0.1865±0.1444
MATERN	0.1504±0.0011	0.0442 ±0.0033
PERIODIC	0.2500±0.0088	0.1149±0.0078
SPECTRAL	0.1549±0.0106	0.0533±0.0075

Figure 2 demonstrates the training and test set generation. The sphere on the left-hand side displays the exp-cos function of equation 14, from which test points are drawn. The sphere on the right-hand side displays a noisy version of the exp-cos function, with noise drawn from $\mathcal{N}(\mu = 0, \sigma = 0.2)$; training points are simulated from such realizations.

Table 3 provides an empirical comparison of the kernels involved by showing numerical summaries of predictive performance. For each kernel, the mean MAE, mean MSE and associated standard errors across the four test sets are tabulated. In this GP regression experiment, the PGF kernel outperforms the RBF kernel in terms of MAE and MSE. This observation confirms empirically proposition 3.3, according to which PGF kernels form a superset of RBF kernels. Moreover, the PGF kernel attains the lowest MAE and second lowest MSE across all kernels. The observed advantage of the PGF kernel is supported by the different scaling of error metrics, indicated by the reported standard errors. Notably, only the PGF and Matern kernels exhibit comparable predictive performance, outperforming the RBF, periodic and spectral mixture kernel.

4.3. Deep Kernel Learning

As a last example, the supervised learning problem of multi-class classification on the hypersphere is considered. To this end, the hyperspherical Thomas process (Thomas, 1949) on \mathbb{S}^h is used. The hyperspherical Thomas process is conditioned on the number of clusters, given the supervised learning setup.

Data are generated from this doubly stochastic process. First, cluster centers are simulated on the hypersphere uniformly at random. Second, for each cluster, data points are simulated from a von Mises-Fisher distribution whose mean direction is set to be the cluster center. The number of data points per cluster is drawn from a Poisson distribution. Thus, three sets of parameters are involved in the data generation process, namely the intensity λ of the underlying Poisson process, and the mean directions μ and concentration parameters κ of the von Mises-Fisher distributions. Four datasets are simulated this way from the hyperspherical Thomas process. Each of the four datasets is split into two halves to generate four corresponding training and test sets. In this example, the multiclass classification problem involves four clusters, and the parameters are set to $h = 17$, $\lambda = 850$ and $\kappa = (20, 20, 20, 20)$. To give an indication of sample size, the mean number of data points across the four datasets (before being split into training and test sets) is 8147.

A DKL classification model is fitted to the data simulated from the hyperspherical Thomas process. The adopted model is a modification of the DKL framework introduced by Wilson et al. (2016). More specifically, the multilayer perceptron of Liang & Tran-Bach (2021) is used as the neural network component of the DKL model. This choice of representation for the multilayer perceptron is made to map the input data on the unit hypersphere to embeddings on the unit sphere. The embeddings must be on the unit sphere to respect the input requirements for the PGF kernel. The Dirichlet-based GP of Milios et al. (2018) is employed as the GP component of the DKL model. Thus, GP classification is performed through the latter part of the DKL model, using the embeddings as input to the GP. This modified DKL model has been chosen over standalone GP classification for two reasons. First, the DKL model reduces the computational cost of GP classification by embedding the input into a lower-dimensional latent spherical space. Second, these embeddings facilitate explainability, as they constitute latent features in \mathbb{R}^3 that can be visualized.

A predictive performance comparison is made between the PGF kernel and the RBF, Matern and periodic kernel in the context of this DKL example. The PGF kernel with depth $n = 3$ and widths $(m_1, m_2, m_3) = (20, 20, 20)$ is used.

For each kernel, two steps are taken. First, a DKL model is fitted to each training set by running the Adam optimizer for

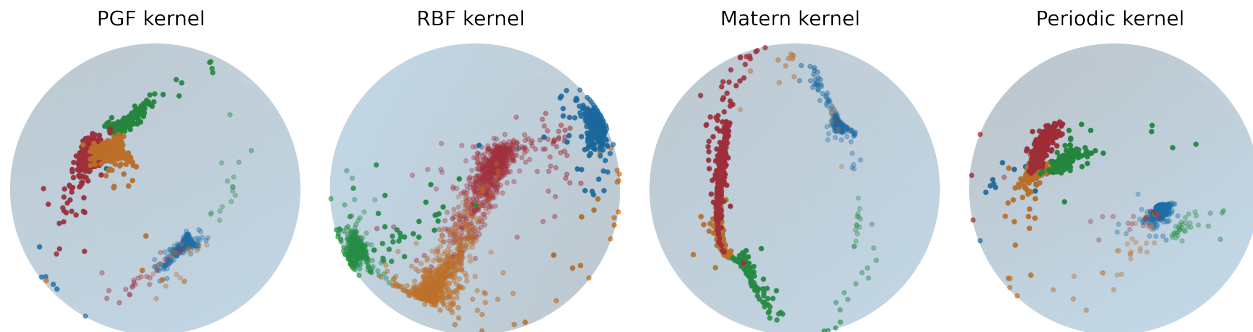


Figure 3. Embeddings in \mathbb{R}^3 generated by training a DKL classification model on a dataset simulated from a hyperspherical Thomas process in \mathbb{R}^{18} . Each of the four spheres displays the embeddings generated by training the DKL model with a different kernel. On each sphere, the four colors of the embeddings represent the four classes of the classification problem.

Table 4. Mean predictive accuracies and standard errors for DKL classification fitted to data, drawn from the hyperspherical Thomas process, using PGF, RBF, Matern and periodic kernels. For each kernel, the mean predictive accuracy and standard error are obtained from four runs (for details, see the main text). The bold font indicates best performance.

KERNEL	ACCURACY (%)
PGF	88.55 ± 4.8772
RBF	88.30 ± 5.1280
MATERN	88.10 ± 5.0961
PERIODIC	88.27 ± 4.9245

the same number of iterations (500). Second, predictions are made and error metrics are computed on the corresponding test set.

Figure 3 shows the embeddings generated by fitting the DKL model to one of the training sets. The embeddings produced by each kernel are visualized on the unit sphere. On each displayed sphere, the four colors of the embeddings represent the four classes of the classification problem. The PGF kernel yields more distinct clusters of embeddings than the RBF kernel, and more generally than the other kernels.

Table 4 summarizes the predictive performance of the four compared kernels. For each kernel, the table shows the mean predictive accuracy and its standard error across the four test sets. In this DKL classification experiment, the PGF kernel outperforms the RBF kernel in terms of predictive accuracy. Moreover, the PGF kernel achieves the highest predictive accuracy among the four kernels.

So, the predictive performance of table 4 and the clustering visualization of figure 3 demonstrate the superiority of the PGF kernel in this DKL example. However, the standard errors of table 4 indicate that the observed differences in performance between the four kernels seem negligible.

5. Discussion and Future Directions

This paper has introduced the family of PGF kernels. Due to their parameterization, PGF kernels replace kernel hyperparameter optimization with a semi-parametric learning task. Since PGF kernels generalize RBF kernels, the former provide an alternative to the latter in the case of spherical data.

Several directions for theoretical research arise. PGF kernels satisfying the closure property may be used to approximate arbitrary PGF kernels; characterizing the quality of such an approximation is an open problem. This approximation is beneficial in two ways. First, PGF kernels with or without the closure property lead to non-parametric or semi-parametric learning tasks, respectively. For example, the fewer parameters of a PGF kernel that satisfies the closure property can be treated as hyperparameters in a non-parametric setting. Thus, PGF kernels with the closure property, if used as proxies to PGF kernels without the closure property, can simplify the learning task. Second, the closure property substantially reduces the computational cost.

Another theoretical problem is to identify conditions on the parameters of a PGF kernel so that the kernel is optimal for certain classes of data or learning tasks. In other words, the question becomes how to select an optimal PGF for a given dataset under the PGF kernel setup.

Spherical data analysis gives rise to future applications of PGF kernels. For instance, simulations of partial differential equations on a sphere, such as Boussinesq convection on a spherical shell or viscous shallow-water motion on a sphere, are computationally expensive. GP emulators with PGF kernels can be used to reduce computational cost. As another example, PGF kernels can find applications in earth data science, including air temperature forecasting and ocean surface topography interpolation.

Acknowledgements

This material is based upon work supported by the Google Cloud Research Credits program with the award GCP19980904. The authors would like to thank Devan-shu Agrawal, Serik Sagitov and Umberto Noe for useful discussions.

References

- Alsmeyer, G. Linear fractional Galton–Watson processes in random environment and perpetuities. *Stochastics and Quality Control*, 2021.
- Daniely, A., Frostig, R., and Singer, Y. Toward deeper understanding of neural networks: the power of initialization and a dual view on expressivity. In *Advances in Neural Information Processing Systems*, volume 29. Curran Associates, Inc., 2016.
- Fischer, H. *A history of the central limit theorem: From classical to modern probability theory*. Springer, 2011.
- Gardner, J. R., Pleiss, G., Bindel, D., Weinberger, K. Q., and Wilson, A. G. GPyTorch: Blackbox matrix-matrix Gaussian process inference with GPU acceleration. In *Advances in Neural Information Processing Systems*, 2018.
- Grimmett, G. and Stirzaker, D. *Probability and random processes*. Oxford university press, fourth edition, 2020.
- Guinness, J. and Fuentes, M. Isotropic covariance functions on spheres: Some properties and modeling considerations. *Journal of Multivariate Analysis*, 143:143–152, 2016.
- Harris, T. E. *The theory of branching processes*. Springer-Verlag, 1963.
- Kersting, G. and Vatutin, V. *Discrete time branching processes in random environment*. John Wiley and Sons, 2017.
- Kozlov, M. V. On the asymptotic behavior of the probability of non-extinction for critical branching processes in a random environment. *Theory of probability and its applications*, 21(4):791–804, 1977.
- Lei, H., Akhtar, N., and Mian, A. Octree guided CNN with spherical kernels for 3D point clouds. In *2019 IEEE/CVF Conference on Computer Vision and Pattern Recognition (CVPR)*, pp. 9623–9632, 2019.
- Liang, T. and Tran-Bach, H. Mehler’s formula, branching process, and compositional kernels of deep neural networks. *Journal of the American Statistical Association*, pp. 1–14, 2021.
- Marques, R., Bouville, C., and Bouatouch, K. Gaussian process for radiance functions on the \mathbb{S}^2 sphere. *Computer Graphics Forum*, 41(6):67–81, 2022.
- Milios, D., Camoriano, R., Michiardi, P., Rosasco, L., and Filippone, M. Dirichlet-based Gaussian processes for large-scale calibrated classification. In *Proceedings of the 32nd International Conference on Neural Information Processing Systems, NIPS’18*, pp. 6008–6018. Curran Associates Inc., 2018.
- Pennington, J., Yu, F. X. X., and Kumar, S. Spherical random features for polynomial kernels. In *Advances in Neural Information Processing Systems*, volume 28. Curran Associates, Inc., 2015.
- Rasmussen, C. E. and Williams, C. K. *Gaussian processes for machine learning*. MIT Press, 2005.
- Sagitov, S. and Lindo, A. *A special family of Galton-Watson processes with explosions*, pp. 237–254. Springer International Publishing, 2016.
- Seal, H. L. The historical development of the use of generating functions in probability theory. *Mitt Verein Schweiz Versich Math*, 49:209–228, 1949.
- Smola, A., Óvári, Z., and Williamson, R. C. Regularization with dot-product kernels. In *Advances in Neural Information Processing Systems*, volume 13. MIT Press, 2001.
- Thomas, M. A generalization of Poisson’s binomial limit for use in ecology. *Biometrika*, 36(1/2):18–25, 1949.
- Wilson, A. G., Hu, Z., Salakhutdinov, R., and Xing, E. P. Deep kernel learning. In *Proceedings of the 19th International Conference on Artificial Intelligence and Statistics*, volume 51 of *Proceedings of Machine Learning Research*, pp. 370–378. PMLR, 2016.
- Zhao, C. and Song, J. S. Exact heat kernel on a hypersphere and its applications in kernel SVM. *Frontiers in Applied Mathematics and Statistics*, 4, 2018.

A. PGFs with Explicit Iterations

This appendix recaps on the definitions of Harris, linear fractional and θ PGFs. Definition A.3 reproduces the definition of θ PGFs, as introduced in Sagitov & Lindo (2016).

Definition A.1. A Harris PGF with parameters c and r is defined as

$$g(s) = (cs^{-r} - (c-1))^{-\frac{1}{r}}, \quad s \in [-1, 1], \quad (15)$$

where $r \in \mathbb{N}$ and $c > 1$.

Definition A.2. A linear fractional PGF with parameters a and b is defined as

$$g(s) = 1 - (a(1-s)^{-1} + b)^{-1}, \quad s \in [-1, 1], \quad (16)$$

where $a > 0$, $b > 0$, and $a + b \geq 1$.

Definition A.3. For $\theta \in (-1, 0) \cup (0, 1]$, consider the PGF

$$g(s) = r - (a(r-s)^{-\theta} + c)^{-1/\theta}, \quad \theta \in (-1, 0) \cup (0, 1]. \quad (17)$$

It is assumed that the parameters θ , a , c and r satisfy one of the three options

$$\begin{aligned} \theta \in (0, 1], & \quad a \geq 1, \quad c > 0, & \quad r = 1, \\ \theta \in (-1, 0) \cup (0, 1], & \quad a \in (0, 1), \quad c = (1-a)(1-q)^{-\theta}, \quad q \in [0, 1], & \quad r = 1, \\ \theta \in (-1, 0) \cup (0, 1], & \quad a \in (0, 1), \quad c = (1-a)(r-q)^{-\theta}, \quad q \in [0, 1], & \quad r > 1. \end{aligned}$$

For $\theta = 0$, consider the PGF

$$g(s) = r - (r-q)^{1-a}(r-s)^a, \quad \theta = 0. \quad (18)$$

It is assumed that parameters q and r satisfy one of the two options

$$\begin{aligned} q \in [0, 1), \quad r = 1, \\ q \in [0, 1], \quad r > 1. \end{aligned}$$

For $\theta = -1$, consider the PGF

$$g(s) = as + (1-a)q, \quad \theta = -1. \quad (19)$$

It is assumed that $a \in (0, 1)$ and $q \in [0, 1]$.

For each of the three cases $\theta \in (-1, 0) \cup (0, 1]$, $\theta = 0$ and $\theta = -1$, the corresponding PGF given by equation 17, 18 and 19 is called a θ PGF.

For any fixed choice of θ , a , c and r , an n -fold iteration of the corresponding θ PGF yields a θ PGF. Thus, an n -fold iteration of a θ PGF is expressed in closed form. The families of θ PGFs and of Harris PGFs (Harris, 1963, p. 10) are the only two known PGF families with explicit n -fold iterations.

B. PGF Kernels Satisfying the Closure Property

This appendix establishes some properties of PGF kernels that arise from compositions of Harris, linear fractional and θ kernels. Proposition B.1 states a symmetry property of the Harris kernel. Propositions B.2, B.3 and B.4 state the corresponding closure property of the Harris kernel, linear fractional kernel and PGF kernels arising from n -fold iterations of θ PGFs. The appendix concludes with the proofs of propositions 3.9 and 3.10.

Proposition B.1. For any even r and any $(x, z) \in \mathbb{S}^h \times \mathbb{S}^h$, the Harris kernel satisfies

$$\mathcal{H}_{c,r}(x, z) = \mathcal{H}_{c,r}(-x, z) = \mathcal{H}_{c,r}(x, -z). \quad (20)$$

Proof. Equation 20 follows from equation 10 for even r . □

Proposition B.2. For any $n \in \mathbb{N}$, let $\mathcal{K}[g_1, \dots, g_n]$ be an n -depth PGF kernel, where g_i , $i = 1, \dots, n$, is a Harris PGF with parameters c_i and r . The n -depth PGF kernel $\mathcal{K}[g_1, \dots, g_n]$ is the Harris kernel $\mathcal{H}_{w_n, r}$ where $w_n = \prod_{i=1}^n c_i$.

Proof. Equation 20 follows from equation 10 for even r . □

Proof. The proposition will be proved by induction. For $n = 1$, according to equations 2, 15 and 10, notice that

$$\mathcal{K}[g_1](x, z) = g_1(\rho(x, z)) = \mathcal{H}_{w_1, r}(x, z).$$

Assuming that

$$\mathcal{K}[g_1, \dots, g_n](x, z) = (w_n \rho(x, z)^{-r} - (w_n - 1))^{-\frac{1}{r}} = \mathcal{H}_{w_n, r}(x, z) \quad (21)$$

holds for $n = j$, it will be shown that it also holds for $n = j + 1$. To this end,

$$\begin{aligned} \mathcal{K}[g_1, \dots, g_{j+1}](x, z) &= g_{j+1} \circ g_j \circ \dots \circ g_1(\rho(x, z)) && \text{See equation 2} \\ &= g_{j+1} \circ \mathcal{K}[g_1, \dots, g_j](x, z) && \text{See equation 2} \\ &= g_{j+1} \left((w_j \rho(x, z)^{-r} - (w_j - 1))^{-\frac{1}{r}} \right) && \text{See equation 21} \\ &= (w_{j+1} \rho(x, z)^{-r} - (w_{j+1} - 1))^{-\frac{1}{r}}, && \text{See equation 15} \end{aligned}$$

which completes the proof. □

Proposition B.3. For any $n \in \mathbb{N}$, let $\mathcal{K}[g_1, \dots, g_n]$ be an n -depth PGF kernel, where g_i , $i = 1, \dots, n$, is a linear fractional PGF with parameters a_i and b_i . The n -depth PGF kernel $\mathcal{K}[g_1, \dots, g_n]$ is the linear fractional kernel \mathcal{F}_{u_n, v_n} , where $u_n = \prod_{i=1}^n a_i$ and $v_n = \sum_{i=1}^n u_{i-1} b_i$.

Proof. The proposition will be proved by induction. For $n = 1$, according to equations 2, 16 and 11, notice that $\mathcal{K}[g_1](x, z) = g_1(\rho(x, z)) = \mathcal{F}_{u_1, v_1}(x, z)$. Assuming that

$$\mathcal{K}[g_1, \dots, g_n](x, z) = 1 - \left(u_n (1 - \rho(x, z))^{-1} + v_n \right)^{-1} = \mathcal{F}_{u_n, v_n}(x, z) \quad (22)$$

holds for $n = j$, it will be shown that it also holds for $n = j + 1$. To this end,

$$\begin{aligned} \mathcal{K}[g_1, \dots, g_{j+1}](x, z) &= g_{j+1} \circ g_j \circ \dots \circ g_1(\rho(x, z)) && \text{See equation 2} \\ &= g_{j+1} \circ \mathcal{K}[g_1, \dots, g_j](x, z) && \text{See equation 2} \\ &= g_{j+1} \left(1 - \left(u_j (1 - \rho(x, z))^{-1} + v_j \right)^{-1} \right) && \text{See equation 22} \\ &= 1 - \left(u_{j+1} (1 - \rho(x, z))^{-1} + v_{j+1} \right)^{-1}, && \text{See equation 16} \end{aligned}$$

which completes the proof. □

Proposition B.4. A PGF kernel that arises from the n -fold iteration of a θ PGF expresses in closed form according to one of the nine cases of table 5 depending on the values of parameters θ, a, q, c, r of the θ PGF.

Proof. Closed-form expressions for n -fold iterations of a θ PGF f are provided in Sagitov & Lindo (2016, section 4). Thus, table 5 follows. □

Proof of proposition 3.9. The proposition will be proved by induction, starting from definition 3.1. For $n = 1$, notice that $\mathcal{K}[g_1](x, z) = g_1(\rho(x, z)) = \mathcal{T}_{\theta, c_1}(x, z)$. Assuming that equation 12 holds for $n = j$, it will be shown that it also holds for

Probability-Generating Function Kernels for Spherical Data

Case	$\mathcal{K}[(g)_n]$	θ	a	q, c	r
1	$1 - (a^n(1 - \rho)^{-\theta} + (a^n - 1)c)^{-1/\theta}$	$(0, 1]$	$(1, \infty)$	$(0, \infty)$	1
2	$1 - ((1 - \rho)^{-\theta} + nc)^{-1/\theta}$	$(0, 1]$	1	$(0, \infty)$	1
3	$1 - (a^n(1 - \rho)^{-\theta} + (1 - a^n)(1 - q)^{-\theta})^{-1/\theta}$	$(0, 1]$	$(0, 1)$	$[0, 1]$	1
4	$1 - (1 - q)^{1-a^n}(1 - \rho)^{a^n}$	0	$(0, 1)$	$[0, 1]$	1
5	$1 - (a^n(1 - \rho)^{ \theta } + (1 - a^n)(1 - q)^{ \theta })^{1/ \theta }$	$(-1, 0)$	$(0, 1)$	$[0, 1]$	1
6	$a^n\rho + (1 - a^n)q$	-1	$(0, 1)$	$[0, 1]$	1
7	$r - (a^n(r - \rho)^{-\theta} + (1 - a^n)(r - q)^{-\theta})^{-1/\theta}$	$(0, 1]$	$(0, 1)$	$[0, 1]$	$(1, \infty)$
8	$r - (r - q)^{1-a^n}(r - \rho)^{a^n}$	0	$(0, 1)$	$[0, 1]$	$(1, \infty)$
9	$r - (a^n(r - \rho)^{ \theta } + (1 - a^n)(r - q)^{ \theta })^{1/ \theta }$	$(-1, 0)$	$(0, 1)$	$[0, 1]$	$(1, \infty)$

Table 5. PGF kernels $\mathcal{K}[(g)_n]$, where g is a θ PGF and $\rho(x, z)$ is the correlation between $x \in \mathbb{S}^h$ and $z \in \mathbb{S}^h$.

$n = j + 1$. To this end,

$$\begin{aligned}
 \mathcal{K}[g_1, \dots, g_{j+1}](x, z) &= g_{j+1} \circ g_j \circ \dots \circ g_1(\rho(x, z)) && \text{See equation 2} \\
 &= f_{j+1} \circ \mathcal{K}_{1:j}(x, z) && \text{See equation 2} \\
 &= g_{j+1} \left(1 - \left((1 - \rho(x, z))^{-\theta} + \sum_{i=1}^j c_i \right)^{-\frac{1}{\theta}} \right) && \text{See equation 12} \\
 &= 1 - \left((1 - \rho(x, z))^{-\theta} + \sum_{i=1}^{j+1} c_i \right)^{-\frac{1}{\theta}}, && \text{See equation 17}
 \end{aligned}$$

which completes the proof. □

Proof of proposition 3.10. Taking the limit of equation 12 as n tends to infinity yields equation 13. □